Electronic Supplementary Material (ESI) for Journal of Materials Chemistry A.

Supporting information for

Enhanced peroxymonosulfate-mediated photocatalytic pesticide degradation by a novel stable multi-metal ferrite (Mg, Cu, Fe) anchored on g-C_3N_4

Samaneh Taghilou [1,2], Babak Kakavandi [3], Mohammad Reza Mehrasbi [4], Ali Esrafili [1,2], Emad Dehghanifard [1,2], Majid Kermani [1,2,*], Stefanos Giannakis[5]

[*] *Research Center for Environmental Health Technology, Iran University of Medical Sciences, Tehran, Iran (Email address: majidkermani@yahoo.com).*

[1] *Research Center for Environmental Health Technology, Iran University of Medical Sciences, Tehran, Iran*
[2]*Department of Environmental Health Engineering, School of Public Health, Iran University of Medical Sciences, Tehran, IR, Iran*
[3] *Department of Environmental Health Engineering, Alborz University of Medical Sciences, Karaj, Iran*
[4]*Department of Environmental Health Engineering, School of Public Health, Zanjan University of Medical Sciences, Zanjan, Iran*
[5]*Universidad Politécnica de Madrid, E.T.S. de Ingenieros de Caminos, Canales y Puertos, Departamento de Ingeniería Civil: Hidráulica, Energía y Medio Ambiente, Environment, Coast and Ocean Research Laboratory (ECOREL-UPM), c/Profesor Aranguren, s/n, ES-28040, Madrid, Spain*

Text S1:

2,4-D ($C_8H_6Cl_2O_3$, ≥ 98%), potassium peroxymonosulfate in the form of OXONE® salt ($H_3K_5O_{18}S_4$, 45%), magnesium chloride hexahydrate ($MgCl_2.6H_2O$, 98%), copper(II) chloride dehydrate ($CuCl_2.2H_2O$, 97.5%), iron(II) chloride hexahydrate ($FeCl_3.6H_2O$, 99%), melamine ($C_3H_6N_6$, ≥ 99%), p-benzoquinone ($C_6H_4O_2$, ≥ 98%), di-ammonium oxalate ($(NH_4)_2C_2O_4.H_2O$, ≥ 99%), anhydrous ethyl alcohol (C_2H_5OH, 99.9%), sodium azide (NaN_3, 99%), potassium persulfate ($K_2S_2O_8$, 99%), hydrogen peroxide (H_2O_2, 35%), sodium hypochlorite (NaClO, 10%), sulfuric acid (H_2SO_4, 98%), sodium hydroxide (NaOH, 99%), ammonia (NH_3, 25%), sodium chloride (NaCl, 99%), sodium carbonate (Na_2CO_3, 99%), sodium bicarbonate ($NaHCO_3$, 99%), sodium nitrate ($NaNO_3$, 99%), sodium sulfate (Na_2SO_4, 99%),

potassium dihydrogen phosphate (K2HPO4, 99%), potassium chloride (KCl, 99%), Methyl methyl alcohol, and water were acquired from SAMCHUN South Korea company in HPLC grade.

Table S1:

Physiochemical properties of the real samples.

Parameter	Average value		
	Tap water (TW)	Treated wastewater (TWW)	River water (RW)
COD (mg/L)	-	21	-
BOD_5 (mg/L)	-	10	-
TSS (mg/L)	-	15	-
TDS (mg/L)	574		
pH	8.29	7.26	7.85
NTU	0.19	3	2.5
EC (µmho/cm)	820	-	380
Hardness (mg/L as CaCo3)	318	-	-

Text S2:

For GCN preparation, a certain amount of melamine was first placed inside a porcelain crucible and in an oven at 550 °C for 2.5~3 hours. The samples were placed in an oven, cooled to ambient temperature, and crushed using a mortar (1). In the conventional method, 1.015 g of $CuCl_{2.2}H_2O$ (0.005 mol), 0.585 g of $MgCl_2.6H_2O$ (0.005 mol), and 5.41 g of $FeCl_3.6H_2O$ (0.02 mol) were dissolved in 50 mL of DI water. The blend was vigorously stirred at 600 rpm for 15 min by using a mechanical mixer. Subsequently, ammonia solution (5 M) was gradually added to the mixture to increase the pH of the solution to approximately 9–10. The blend was then heated to 80 °C and stirred continuously for 1 h. The mixture was then brought to room temperature, and the resulting solid was cleaned through multiple washes with distilled water and ethanol and then filtered using

a vacuum pump. The purified residue was dried at 150 °C for 8 h in an oven and subsequently calcined at 900 °C for 3 h in a furnace (2). GCN@MCF was prepared using the method described above for MCF. To determine the optimum MCF mass for the 10%-GCN@MCF structure, 10, 20, 30, and 50 wt. % GCN were used during the synthesis of the MCF nanoparticles.

Text S3:

To investigate the structural characteristics and crystalline phases, X-ray diffraction (XRD, Philips PW1730) was performed in the 2θ scanning range of 10–80° at 25 °C (λ = 1.54 Å). The surface morphology, size, and structure of the samples were analyzed using field-emission scanning electron microscopy (FESEM; TESCAN MIRA3). Energy-dispersive X-ray spectroscopy (EDX) and energy-dispersive spectroscopy (EDS, ARYA Electron Optic) were employed to determine the elemental composition of the samples. Transmission electron microscopy (TEM, Philips EM 208S) images were obtained to characterize the size and shape of the prepared nanoparticles. To ascertain the specific surface areas of the catalysts, N2 adsorption/desorption isotherms were recorded using a BELSORP Mini II instrument based on the Brunauer–Emmett–Teller (BET) theory. To evaluate the volume and average diameter of the pores of the catalyst, Barrett-Joyner-Halenda (BJH) analysis was employed, which was derived from the N_2 adsorption/desorption curves. The optical characteristics of the catalysts were assessed using UV–Vis diffuse reflectance spectroscopy (DRS) (Thermo Biomate5). Photoluminescence (PL, CARY ECLIPSE) spectra were recorded at λ_{ex} between 300-800 nm, to understand the separation and recombination of photoinduced e-/h+ pairs on the synthesized samples. For PL analysis, the excitation wavelength was set to 360 nm. The magnetic hysteresis loops of the samples were measured using a vibrating sample magnetometer (VSM; MDKB) at 25 °C under a magnetic field of ±30 kOe. Electrochemical impedance spectroscopy (EIS, Metrohm DropSens, μStat-i 400s) was employed to assess the resistance, recombination, and transmission rate of charge carriers

(e-/h+) on the surface of the photocatalyst semiconductors. The EIS analysis was conducted in a 0.5 M sodium sulfate electrolyte, 0.01-100 a frequency range, and an AC voltage of 10 mV. X-ray photoelectron spectroscopy (XPS; Bes Tek, Germany) measurements were carried out in a vacuum of 10-10 mbar, an X-ray anode of Al, and a kα Al of 1486.6 eV to analyze the surface chemical composition and electronic state of the samples. Photocurrents were measured using an electrochemical analyzer (0.5 V AC voltage, 0.5 M sodium sulfate electrolyte) to determine the transient optical current of the catalysts. The potential of zero charge (pHzpc) of the 10%-GCN@MCF was measured using the pH drift method (3). For this purpose, the starting pH of a set of 0.1 M KCl solutions was adjusted to 2, 4, 6, 7, 8, and 10 using 0.1 M NaOH or HCl. The catalyst (50 mg) was added to 50 mL of KCl solution at varying pH levels. The final solution pH was measured after 24 h. The pH_{zpc} of the catalyst was derived from the correlation between the initial and final pH values of the solution.

Text S4:

A stock solution was prepared by adding a predetermined amount of 2,4-D to the DI water. The pH of the reaction mixture was adjusted with HCl (0.1 M) and NaOH (0.1 M). Before initiating each test, the lamp underwent a 30-min warm-up period to establish stable visible-light emission. In this process, a defined amount of catalyst was added to the samples and vigorously shaken using a mechanical shaker at a constant speed of 2000 rpm for 30 min, ensuring adsorption-desorption equilibrium. Subsequently, the solution was transferred into the reactor, PMS was added, and the mixture was mechanically stirred at 2000 rpm for 120 min. At specified time intervals, the samples were extracted and promptly subjected to a magnetic field, and the supernatant was analyzed by high-performance liquid chromatography (HPLC) to quantify the residual concentrations of 2,4-D. The 2,4-D degradation efficiency and mineralization degree were determined using the Eq. (1) and (2), respectively. To prevent an increase in the temperature

of the solution and evaporation of the samples, a water jacket and a ventilation device were placed close to the reactor. The groups of photocatalytic tests performed included i) operational parameters (%GCN, pH, [catalyst], [PMS], and [2,4-D]); ii) matrix effect (co-existing ions and matrix source); iii) runs with scavengers; iv) catalyst robustness; v) 2,4-D degradation pathways; and vi) toxicity and biodegradability assays. All experiments were performed at least three times, and the mean values were calculated. The standard deviation remained below 5%, indicating high reproducibility.

Key operation parameters such as mass ratios of GCN (10, 20, 30, and 50 %W), pH (3.0-11.0), catalyst dosage (0.1-0.5 g/L), PMS dose (2-6 mM), and initial concentration of 2,4-D (5-30 mg/L) were optimized for the GCN@MCF/PMS/VL process within 120 min of reaction. After optimization, comparative tests were performed to evaluate the degradation kinetics, effect of coexisting anions (e.g., chloride (Cl^-), nitrate (NO_3^-), carbonate (CO_3^{2-}), bicarbonate (HCO_3^-), sulfate (SO_4^{2-}), and phosphate (PO_4^{3-})), and scavengers (e.g., benzoquinone (BQ), tert-butyl alcohol (t-BuOH), sodium azide (SA), ammonium oxalate (AO), and methanol (MeOH)) on process efficiency. Thereafter, the reusability, stability, and mineralization tests were conducted over six consecutive runs. Furthermore, the intermediate byproducts of 2,4-D degradation were identified to propose plausible degradation pathways. Finally, toxicity and biodegradability of the reaction solutions were evaluated.

$$\%Degradation = \left[\frac{C_0 - C_t}{C_0}\right] \times 100\% \quad (1)$$

Where C_t and C_o are the 2,4-D concentrations at time t and at the initial time, respectively. The mineralization efficiency of the system was calculated using the following equation:

$$Mineralization\ degree\ (\%) = \left[\frac{TOC_0 - TOC_t}{TOC_0}\right] \times 100\% \quad (2)$$

Where TOC_t and TOC_0 are the total organic carbon concentrations of the solution at time t and the initial time, respectively.

Text S5:

LC system (Waters Alliance 2695) conditions: solvent A (ACN + 0.1% Formic Acid 70%), solvent B (H_2O + 0.1% Formic Acid 30%), column model C18 5μ, 4.6×120 mm, temperature 35 °C, flowrate 0.3 mL/min, injection volume 10 μL. The MASS system (Micromass Quattro micro API) conditions: ESI -/+, cone voltage 20 V, capillary voltage 4 kV, extractor 2 V, RF lens 0.1 V, gas nebulizer N_2 (grade 5), flow gas 250 L/h; source temperature 120 °C, desolation temperature 350 °C.

Text S6:

In the photocatalytic processes, the pH of the solution plays a pivotal role, exerting influence on multiple facets, such as the surface charge of the photocatalyst, ionization of the organic pollutant, activity of the oxidant, formation of active radicals, specific surface area of the catalyst, chemical properties of the pollutant, and kinetics of the reaction (4, 5). Fig. S1a presents the removal efficiency of 2,4-D by 10%-GCN@MCF/PMS/VL in the pH range of 3-11. The solution pH from 3 to 7 degradation efficiency of 2,4-D increased from 28.0% to 67.4%. However, the degradation efficiency declined considerably at higher pH values of 7 and reached 18.3% at pH 11. Given that the pKa of 2,4-D is 2.64, 2,4-D becomes negatively charged when the pH surpasses 2.64 (6, 7). In contrast, the point of zero charge (pHzpc) of the as-prepared 10%-GCN@MCF is 7, as shown in Fig. S1b. This means that the surface of the catalyst is positively charged when the solution pH is below pH_{zpc}, and negatively charged at a pH higher than pH_{zpc} (8). Hence, electrostatic interactions play a significant role in influencing the adsorption between the catalyst and

contaminants when the solution pH is between the pKa values of 2,4-D and pHzpc (7, 9). Both extremely alkaline and acidic environments resulted in decreased photocatalytic activity, according to Eq. 3-6 (10).

$$SO_4^{\bullet -} + H^+ + e^- \rightarrow HSO_4^- \quad (3)$$

$$HO^\bullet + H^+ + e^- \rightarrow H_2O \quad (4)$$

$$SO_4^{\bullet -} + OH^- \rightarrow HO^\bullet + SO_4^{2-} \quad (5)$$

$$SO_4^{\bullet -} + H_2O \rightarrow HO^\bullet + HSO_4^- \quad (6)$$

Under acidic conditions, the reduced removal is attributed to the competitive interaction between H^+ ions and cationic 2,4-D, along with repulsive forces between the cations of the contaminant and positively charged sites (11). Another reason is that the catalyst can break up in extremely acidic or alkaline media (12). Therefore, a pH level of 7 was found as the optimal condition for eliminating 2,4-D using 10%-GCN@MCF during 120 min reaction time with 67.4% removal and 0.0102 min^{-1}.

The amount of catalyst used plays a crucial role in heterogeneous catalytic reactions for pollutant removal. The effect of 10%-GCN@MCF amount on the removal efficiency of 2,4-D at dosages of 0.1-0.5 g/L and the obtained result is shown in Fig. S1c. The findings indicate that as the catalyst dosage was increased from 0.1 to 0.3 g/L during 120 min, the degradation efficiencies of 2,4-D increased from 40.2% (0.0035 min^{-1}) to 67.4% (0.0102 min^{-1}). This increase can be ascribed to the increased accessibility of the active sites for PMS activation, resulting in the generation of more reactive radical species (13). Conversely, an excessive catalyst dosage exceeding 0.3 g/L led to a reduction in the degradation efficiency (31.7%, 0.0027 min^{-1}). Increasing the catalyst dosage resulted in solution turbidity, which accounted for light scattering and reduced the number of active sites on the catalyst, which diminished the photocatalytic activity (14-17). Consequently, a catalyst load of 0.3 g/L, which yielded the maximum degradation efficiency (67.4%, 0.0102 min-

[1]) over the 120-min reaction period, was deemed as the optimum catalyst dosage for the ongoing optimization of the degradation process in subsequent tests.

PMS concentration is a critical parameter in the quantity of sulfate or hydroxyl radicals generated within the medium (13). The effect of PMS concentration on the performance of the 10%-GCN@MCF/PMS/VL system was investigated at levels of 2-6 mM. Fig. S1d illustrates the progressive degradation of 2,4-D with increasing PMS dosage. This indicates a notable dependence of the efficiency of 10%-GCN@MCF/PMS/VL on the PMS dosage, with an observed enhancement in 2,4-D degradation as the PMS dosage increased. The efficiency of 2,4-D degradation increased proportionally as the PMS dosage increased from 2 mM to 5 mM. Specifically, the degradation efficiency increased from 24.1% at 2 mM (0.0023 min^{-1}) to nearly 95.2% at 5 mM (0.0235 min^{-1}) over a 120 min reaction period. Conversely, concentrations exceeding5 mM led to diminished removal efficiency (0.0108 min^{-1}), as depicted in the inset of Fig. 5d. This phenomenon can be attributed to the adverse impact of PMS concentration exceeding the optimum value, resulting in a reduction in the system's efficacy. This decrease is associated with the reactions between $SO_4^{\bullet-}$ and $^{\bullet}OH$ radicals as well as the self-scavenging effect exerted by excess PMS, according to Eqs. (7-11). The observed decline in removal efficiency at lower PMS dosages can be explained by the availability of an insufficient number of $SO4^{\bullet-}$ radicals within the system. These findings are consistent with previously reported reaction rate constants (13, 14).

$$SO^{\bullet}{}_4^- + {}^{\bullet}OH \rightarrow HSO_4^- + \frac{1}{2}O_2 \quad (7)$$

$$SO^{\bullet}{}_4^- + SO^{\bullet}{}_4^- \rightarrow 2SO^2{}_4^- \; or \; S_2O^2{}_8^- \quad (8)$$

$$^{\bullet}OH + {}^{\bullet}OH \rightarrow H_2O_2 \quad (9)$$

$$HSO_5^- + SO^{\bullet}{}_4^- \rightarrow SO^{\bullet}{}_5^- + SO^2{}_4^- + H^+ \quad (10)$$

$$HSO_5^- + {}^{\bullet}OH \rightarrow SO^{\bullet}{}_5^- + H_2O \text{ or } HSO_4^- + HO_2^{\bullet} \quad (11)$$

Hence, a PMS dosage of 5 mM, which yielded the maximum degradation efficiency (95.2%, 0.0235 min^{-1}) over the 120-min reaction, was deemed as the optimum amount of oxidant loading for the upcoming experiments.

The pollutant concentration is a crucial parameter in wastewater treatment because any given treatment process may have limitations and upper levels of degradation capacity. In Fig. S1e, the impact of initial 2,4-D concentrations on the performance of 10%-GCN@MCF/PMS/VL system has been investigated at levels of 5, 10, 15, 20, and 30 mg/L under optimum conditions (pH= 7, catalyst dosage= 0.3 g/L, and PMS dose= 5 mM). With an increase in the initial 2, 4-D concentration from 5 to 30 mg/L, the reaction rate constant exhibited a gradual deceleration, decreasing from 0.0281 to 0.0073 min^{-1}, and the degradation efficiency decreased substantially from 96.0% to 60.2%. Similar trends have been reported for the catalytic degradation of various contaminants (4, 17-19). At low concentrations of 2,4-D, there was an excess of both the catalyst and PMS, promoting more effective photocatalytic reactions between the 2,4-D molecules and catalyst. Conversely, at higher concentrations, an increased number of molecules in the medium may obstruct the active sites on the catalyst, impeding effective decomposition and consequently leading to diminished system performance. Furthermore, higher concentrations contribute to the generation of more intermediates, intensifying the competition between the target pollutant and reactive species (13). Moreover, as the concentration of 2,4-D increases, the penetration of photons is limited, consequently reducing the interaction between the catalyst and light source required to generate reactive species (14, 16).

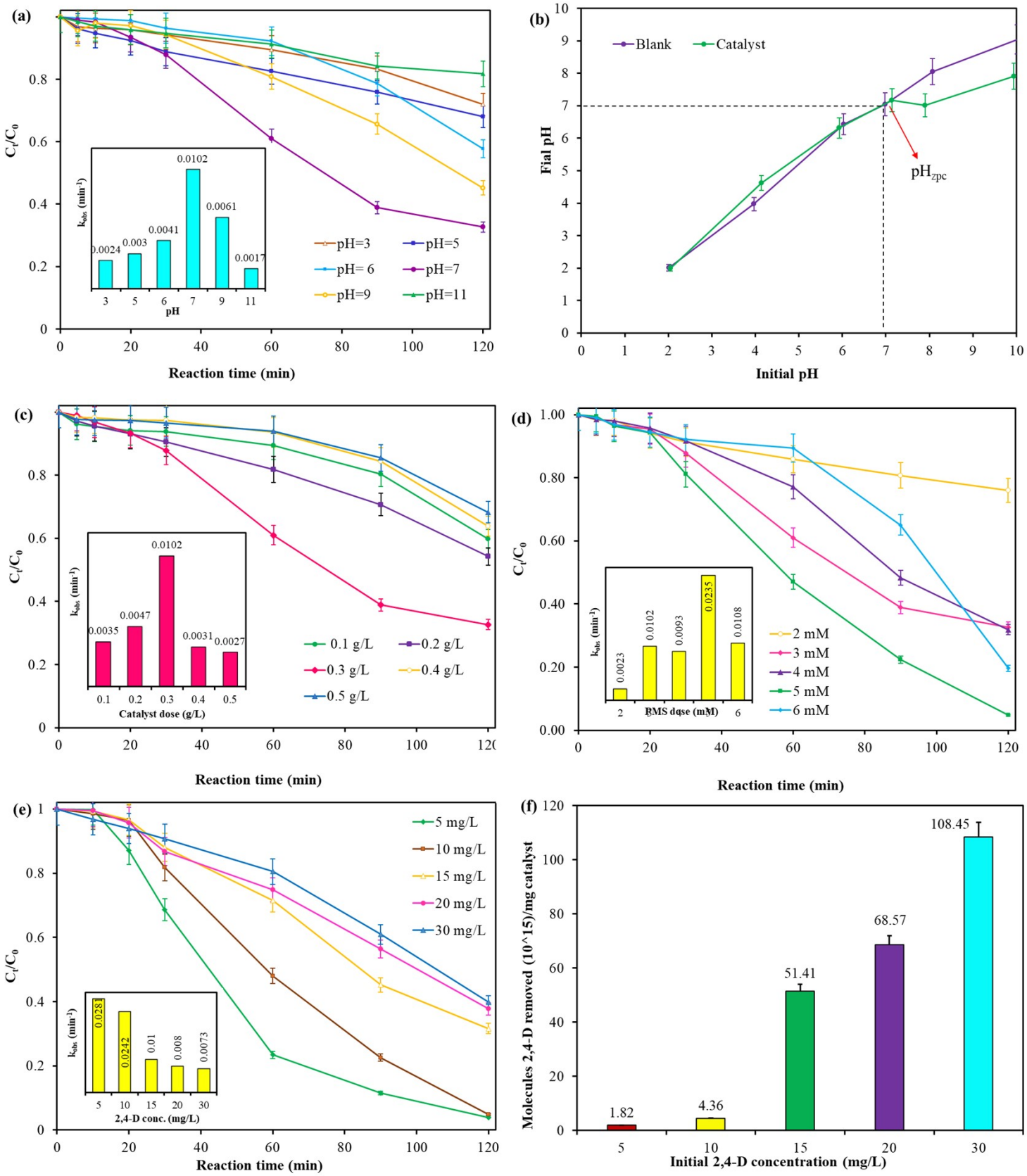
(a)
C_t/C_0
Reaction time (min)
pH=3
pH=5
pH= 6
pH=7
pH=9
pH=11
k_{obs} (min^{-1})
0.0024
0.003
0.0041
0.0102
0.0061
0.0017
pH
(b)
Blank
Catalyst
Fial pH
Initial pH
pH_{zpc}
(c)
C_t/C_0
Reaction time (min)
0.1 g/L
0.2 g/L
0.3 g/L
0.4 g/L
0.5 g/L
k_{obs} (min^{-1})
0.0035
0.0047
0.0102
0.0031
0.0027
Catalyst dose (g/L)
(d)
C_t/C_0
Reaction time (min)
2 mM
3 mM
4 mM
5 mM
6 mM
k_{obs} (min^{-1})
0.0023
0.0102
0.0093
0.0235
0.0108
PMS dose (mM)
(e)
C_t/C_0
Reaction time (min)
5 mg/L
10 mg/L
15 mg/L
20 mg/L
30 mg/L
k_{obs} (min^{-1})
0.0281
0.0242
0.01
0.008
0.0073
2,4-D conc. (mg/L)
(f)
Molecules 2,4-D removed (10^15)/mg catalyst
Initial 2,4-D concentration (mg/L)
1.82
4.36
51.41
68.57
108.45

Fig. S1. Effect of various pH on 2,4-D degradation over 120 min reaction and the values of degradation kinetics constants of 2,4-D (inset) (a), pH_{zpc} of catalyst (b), various catalyst dose (c), various PMS dose (d), various 2,4-D concentrations (e), (f) molecules 2,4-D removed (Reaction conditions: [2,4-D]= 10 ppm, [sample vol.]= 200 cc, [cat.]= 0.3 g/l, [PMS]= 3 mM (for test (e) and (f) was 5 mM), Initial pH= 7 (for test (a) was pH of DI-water), [Temp.]= 25±2 °C).

References:

1. Hassani A, Eghbali P, Ekicibil A, Metin ÖJJoM, Materials M. Monodisperse cobalt ferrite nanoparticles assembled on mesoporous graphitic carbon nitride (CoFe2O4/mpg-C3N4): a magnetically recoverable nanocomposite for the photocatalytic degradation of organic dyes. 2018;456:400-12.
2. Van Tran C, La DD, Hoai PNT, Ninh HD, Hong PNT, Vu THT, et al. New TiO2-doped Cu–Mg spinel-ferrite-based photocatalyst for degrading highly toxic rhodamine B dye in wastewater. 2021;420:126636.
3. Singh KP, Gupta S, Singh AK, Sinha SJJohm. Optimizing adsorption of crystal violet dye from water by magnetic nanocomposite using response surface modeling approach. 2011;186(2-3):1462-73.
4. Yuan X, Duan S, Wu G, Sun L, Cao G, Li D, et al. Enhanced catalytic ozonation performance of highly stabilized mesoporous ZnO doped g-C3N4 composite for efficient water decontamination. 2018;551:129-38.
5. Kakavandi B, Dehghanifard E, Gholami P, Noorisepehr M, MirzaHedayat BJASS. Photocatalytic activation of peroxydisulfate by magnetic Fe3O4@ SiO2@ TiO2/rGO core–shell towards degradation and mineralization of metronidazole. 2021;570:151145.
6. Qiu P, Yao J, Chen H, Jiang F, Xie XJJohm. Enhanced visible-light photocatalytic decomposition of 2, 4-dichlorophenoxyacetic acid over ZnIn2S4/g-C3N4 photocatalyst. 2016;317:158-68.
7. Gu J, Chen H, Jiang F, Wang X, Li LJCEJ. All-solid-state Z-scheme Co9S8/graphitic carbon nitride photocatalysts for simultaneous reduction of Cr (VI) and oxidation of 2, 4-dichlorophenoxyacetic acid under simulated solar irradiation. 2019;360:1188-98.
8. Yuan X, Qin W, Lei X, Sun L, Li Q, Li D, et al. Efficient enhancement of ozonation performance via ZVZ immobilized g-C3N4 towards superior oxidation of micropollutants. 2018;205:369-79.
9. Ghodsi S, Esrafili A, Kalantary RR, Gholami M, Sobhi HRJJoP, Chemistry PA. Synthesis and evaluation of the performance of g-C3N4/Fe3O4/Ag photocatalyst for the efficient removal of diazinon: kinetic studies. 2020;389:112279.

10. Olfatmehr N, Kakavandi B, Khezri SM. Peroxydisulfate activation by enhanced catalytic activity of CoFe2O4 anchored on activated carbon: A new sulfate radical-based oxidation study on the Cefixime degradation. Separation and Purification Technology. 2022;302:121991.
11. Tegenaw AB, Yimer AA, Beyene TTJH. Boosting the photocatalytic activity of ZnO-NPs through the incorporation of C-dot and preparation of nanocomposite materials. 2023;9(10).
12. Zhang L, Cheng H, Zong R, Zhu YJTJoPCC. Photocorrosion Suppression of ZnO Nanoparticles via Hybridization with Graphite-like Carbon and Enhanced Photocatalytic Activity. 2009;6(113):2368-74.
13. Dikdim JMD, Gong Y, Noumi GB, Sieliechi JM, Zhao X, Ma N, et al. Peroxymonosulfate improved photocatalytic degradation of atrazine by activated carbon/graphitic carbon nitride composite under visible light irradiation. 2019;217:833-42.
14. Golshan M, Kakavandi B, Ahmadi M, Azizi MJJohm. Photocatalytic activation of peroxymonosulfate by TiO2 anchored on cupper ferrite (TiO2@ CuFe2O4) into 2, 4-D degradation: Process feasibility, mechanism and pathway. 2018;359:325-37.
15. Kumar A, Sharma G, Naushad M, Ala'a H, Kumar A, Hira I, et al. Visible photodegradation of ibuprofen and 2, 4-D in simulated waste water using sustainable metal free-hybrids based on carbon nitride and biochar. 2019;231:1164-75.
16. Li Z, Ai W, Zhang Y, Zhang J, Liu W, Zhong D, et al. Magnetic carbon nanotube modified S-scheme TiO2-x/g-C3N4/CNFe heterojunction coupled with peroxymonosulfate for effective visible-light-driven photodegradation via enhanced interfacial charge separation. 2023;308:122897.
17. Yang C, Chai H, Xu P, Wang P, Wang X, Shen T, et al. One-step synthesis of a 3D/2D Bi2WO6/g-C3N4 heterojunction for effective photocatalytic degradation of atrazine: Kinetics, degradation mechanisms and ecotoxicity. 2022;288:120609.
18. Bhanvase B, Shende T, Sonawane SJETR. A review on graphene–TiO2 and doped graphene–TiO2 nanocomposite photocatalyst for water and wastewater treatment. 2017;6(1):1-14.
19. Setthaya N, Chindaprasirt P, Yin S, Pimraksa KJPt. TiO2-zeolite photocatalysts made of metakaolin and rice husk ash for removal of methylene blue dye. 2017;313:417-26.